Global Patterns of Spatial and Temporal Variability in Salinity from Multiple Gridded Argo Products

CHAO LIU AND XINFENG LIANG

School of Marine Science and Policy, University of Delaware, Lewes, Delaware

DON P. CHAMBERS

College of Marine Science, University of South Florida, St. Petersburg, Florida

RUI M. PONTE

Atmospheric and Environmental Research, Lexington, Massachusetts

(Manuscript received 29 January 2020, in final form 22 July 2020)

ABSTRACT

Salinity is one of the fundamental ocean state variables and has been used to infer important information about climate change and variability. Previous studies have found inconsistent salinity variations in various objective ocean analyses that are based on the Argo measurements. However, as far as we are aware, a comprehensive assessment of those inconsistencies, as well as robust spatial and temporal features of salinity variability among the Argo-based products, has not been conducted. Here we compare and evaluate ocean salinity variability from five objective ocean analyses that are solely or primarily based on Argo measurements for their overlapping period from 2005 to 2015. We examine the salinity variability at the sea surface and within two depth intervals (0-700 and 700-2000 m). Our results show that the climatological mean is generally consistent among all examined products, although regional discrepancies are evident in the subsurface ocean. The time evolution, vertical structure, and leading EOF modes of salinity variations show good agreement among most of the examined products, indicating that a number of robust features of the salinity variability can be obtained by examining gridded Argo products. However, significant discrepancies in these variations exist, particularly in the subsurface North Atlantic and Southern Oceans. Also, despite the increasing number of Argo floats deployed in the ocean, the discrepancies were not significantly reduced over time. Our analyses, particularly those of the discrepancies between products, can serve as a useful reference for utilizing and improving the existing objective ocean analyses that are based on Argo measurements.

KEYWORDS: Ocean; Salinity; Oceanic variability

1. Introduction

Salinity is one of the fundamental ocean variables that are routinely measured, and variations in salinity have been used extensively in climate studies. First, ocean salinity is strongly impacted by air–sea freshwater exchange, land freshwater discharges, sea ice formation and melting, and ocean dynamics (Rao and Sivakumar 2003; Foltz et al. 2004; Dong et al. 2014; Haumann et al. 2016; Liu et al. 2019). Since salinity is easier to measure than the air–sea freshwater flux, the surface and/or near-surface salinity is often used as a "rain gauge" (Schmitt

 ${\it Corresponding\ author}. \ Chao\ Liu, chaoliu@udel.edu$

2008) for understanding changes in the global water cycle (Hosoda et al. 2009; Helm et al. 2010; Durack et al. 2012; Skliris et al. 2014). Second, despite being an order of magnitude smaller than the thermal contributions (Durack et al. 2014), changes in ocean salinity also contribute to long-term sea level change. On basin scale, in particular, various studies have highlighted the importance of salinity to regional halosteric changes for different time scales (Llovel et al. 2011; von Schuckmann and Traon 2011). For instance, the long-term trends in thermosteric and halosteric changes compensate in the Atlantic Ocean from the 1950s to the 1990s (Levitus et al. 2005).

The description of ocean salinity variations largely relies on available observational datasets (e.g., the World

Ocean Database 2013). Since 2001, the Argo Program, utilizing a large number of autonomous floats, has become one of the essential components of the present global ocean observing system (Argo 2000). This program has allowed for the first time a nearly global sampling of the upper 2000 m ice-free ocean with relatively small bias since about 2005 (Roemmich et al. 2009; Abraham et al. 2013). A number of institutions have developed gridded data products and analyses solely or primarily based on Argo measurements of temperature, salinity, and pressure using different statistical methods. These gridded Argo products have been widely used and are usually considered as the "truth" with some measurement uncertainties (e.g., Chang et al. 2013; Wang et al. 2017).

As many studies have revealed, however, significant discrepancies appear among these gridded Argo products (Lee 2016; Trenberth et al. 2016; Wang et al. 2018). A large portion of these differences relate to the mapping techniques for filling the gaps in time and space (Abraham et al. 2013; Boyer et al. 2016). Moreover, systematic errors also exist in the Argo autonomous measurements (Jayne et al. 2017). For instance, a large portion of real-time profiles might be subject to salinity errors larger than the 0.01 accuracy criterion since 2016 (Roemmich et al. 2019). Substantial variations (>2 mm) in global halosteric time series after 2015 have also been reported (Wang et al. 2017), which, however, are inconsistent with recent Gravity Recovery and Climate Experiment (GRACE)-observed ocean mass changes (Llovel et al. 2019). Since this drifting had happened for several years until it was found within the last two years, it can be a problem for both the real-time and delayedmode data. In this study, due to the reported systematic salinity errors, we will focus on the global and regional salinity changes from 2005 to 2015.

The existence of significant discrepancies among gridded Argo products suggests that estimates of temporal variability and decadal trends in ocean salinity are likely product-dependent. While there have been a number of assessments of the salinity products from various ocean reanalyses and selected objective analyses that are based on Argo measurements (Xue et al. 2012; Chang et al. 2013; Shi et al. 2017; Li et al. 2019), it is necessary to revisit the global- and basin-scale salinity changes on decadal scales and examine the robust features as well as the discrepancies among the Argo products that have been overlooked in the past.

In this study, we conducted an assessment of five selected Argo-based gridded salinity products and revealed what level of consensus and discrepancies can be achieved. The detected uncertainties between different objective analysis (OA) products will further provide an important

basis for future ocean salinity analyses. This paper is organized as follows. Data and methods are described in section 2. An intercomparison of salinity variations at the near surface and within two layers (0–700 and 700–2000 m) is presented in section 3. A summary and discussion of the results are given in sections 4 and 5.

2. Data and methods

a. Gridded salinity datasets

Five Argo-based salinity gridded products are analyzed in this study, including the EN4 ocean objective analysis from the U.K. Met Office (Good et al. 2013), the Roemmich-Gilson Argo climatology from the Scripps Institution of Oceanography (RG; Roemmich and Gilson 2009), the grid point value of the monthly objective analysis using Argo data (MOAA) (Hosoda et al. 2008), the International Pacific Research Center (IPRC) Argo product (IPRC 2019), and the global ocean Barnes objective analysis Argo gridded dataset (BOA; Li et al. 2017). These monthly products have the same horizontal resolution of $1^{\circ} \times 1^{\circ}$ and the overlapping time span of 2005-15. We chose these five gridded products because they are often used in Argorelated studies that included more than one OA product (e.g., Trenberth et al. 2016; Wang et al. 2017, 2018). They are of the same spatial resolution and regularly updated.

For the purpose of global analysis, we will focus on the ice-free open ocean between 60°S and 60°N (Roemmich et al. 2009), although increasing numbers of Argo floats have been deployed in the polar regions (Jayne et al. 2017). We also converted the pressure levels to depths and removed the seasonal signal by fitting and removing annual period sinusoids at each grid point, which provides similar results to those obtained by removing a climatological seasonal cycle (not shown).

Although the discrepancies among the five products cannot reveal any common errors (e.g., drift in salinity observations), they can reveal uncertainty that is caused by different center-specific processes, including mapping methods, data editing, and additional non-Argo data. One of the major differences among the products is that IPRC, RG, and BOA only utilize the temperature and salinity measurements from Argo, while EN4 and MOAA include other data such as from mooring arrays and ship-based observations. These two datasets are also the only ones that used a pre-Argo baseline climatology, making it difficult to differentiate the associated discrepancies and identify the actual sources (i.e., from the climatology or the raw data). However, since profile data from Argo substantially outnumber other forms of

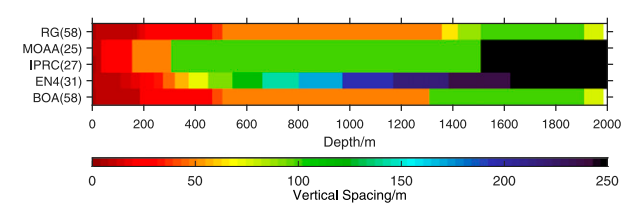


FIG. 1. Vertical grids of the selected gridded products. The number of levels (from the sea surface to 2000 m) for each product is labeled in parentheses.

observations since the early 2000s (Durack 2015), differences in data sources are initially considered as an insignificant factor in the observed discrepancies on the global and basin scales.

In comparison, prior studies show that the mapping methods are a major source of the discrepancies in the gridded products (Boyer et al. 2016). Of the selected five products, BOA uses objective interpolation technique based on Barnes successive correction method (Barnes 1964), while IPRC uses a variational analysis technique (IPRC 2019), which includes calculated dynamic height from satellite data. The other three products are all based on optimal interpolation methods using slightly different methodology and covariance functions (Hosoda et al. 2008; Roemmich and Gilson 2009; Good et al. 2013). As already mentioned, EN4 and MOAA also use pre-Argo baseline climatology [World Ocean Atlas (WOA) 1998 and 2001, respectively whereas others are more recent.

In addition, the vertical grids of salinity profiles vary among the five objective analyses (Fig. 1). As most Argo data are only available in the upper 2000 m, Argo-only datasets (i.e., BOA, RG, and IPRC) have a lower limit around 2000 m. BOA and RG have the highest number of vertical layers and almost identical spacing. Meanwhile, EN4, which provides full depth data, has a similar number of layers to MOAA and IPRC in the upper 2000 m, but most of its layers are concentrated in the top 300 m. Such differences will also contribute to the overall discrepancies (e.g., Toyoda et al. 2017). While this study is mostly focused on vertically averaged layers, the effects of different vertical spacing are also briefly discussed [see section 3b(1)].

b. Comparison strategy

Many studies have found substantial variability and change in ocean salinity in the upper 700 m of the global ocean (e.g., Boyer et al. 2005; Durack and Wijffels 2010; Shi et al. 2017). Basin-scale salinity changes are also found in the deeper ocean (below 700 m), which are associated with density compensation, circulation

changes, and water mass changes (e.g., Curry et al. 2003; Durack et al. 2014; Purkey et al. 2014; Storto et al. 2017). To be consistent with the previous studies, we will examine salinity variations on three depth intervals: the near surface (the vertical average of the top 20 m), 0-700 m, and 700-2000 m.

The ensemble mean (S^{ESM}) and ensemble spread [S^{SPD} ; modified from Balmaseda et al. (2015), Shi et al. (2017), and Xue et al. (2017)] are used to analyze the agreements and disagreements of the five gridded products. At each grid point, S^{ESM} is given by

$$S^{\text{ESM}} = \frac{1}{N} \sum_{n=1}^{N} S_n,$$
 (1)

where N is the total number of Argo products (N = 5), and S_n represents the salinity from individual objective analyses at each time and space grid point (e.g., BOA, IPRC). The averaging involved in $S^{\rm ESM}$ will diminish random and quasi-random errors among the datasets (Balmaseda et al. 2015).

The ensemble spread of the gridded Argo products about the corresponding S^{ESM} is calculated as

$$S^{\text{SPD}} = \sqrt{\frac{1}{N} \sum_{n=1}^{N} (S_n - S^{\text{ESM}})^2}.$$
 (2)

The difference of each product from the ensemble mean is also calculated, and the largest difference (absolute value) among all products is recorded as the "largest deviation" ($S^{\rm LDT}$). Values of $S^{\rm LDT}$ and $S^{\rm SPD}$ reflect the uncertainties that are mostly induced by different mapping methods, baseline climatology, and vertical resolutions. While we cannot directly tell the origin of the discrepancies solely from $S^{\rm LDT}$ and $S^{\rm SPD}$, such information can be inferred by comparing the products in groups based on their common techniques. Low $S^{\rm SPD}$ indicates the results are robust (i.e., products are similar among themselves), and $S^{\rm LDT}$ shows the product that deviates the most from $S^{\rm ESM}$.

Here we consider $S^{\rm LDT}$ in addition to $S^{\rm SPD}$ to account for the fact that we have a small number of samples (N=5) and the standard deviation does not likely reflect the full distribution. Identifying products associated with the largest deviations will detect significant outliers that may not be apparent in the standard deviation value due to clustering in some of the analyses. In addition, since not all the datasets provide a corresponding error matrix (e.g., BOA, IPRC), we assumed that these Argo-based analyses are of similar quality when calculating $S^{\rm ESM}$ and $S^{\rm SPD}$ (Balmaseda et al. 2015). It should be noted that neither the individual Argo products nor $S^{\rm ESM}$ should be simply considered as an

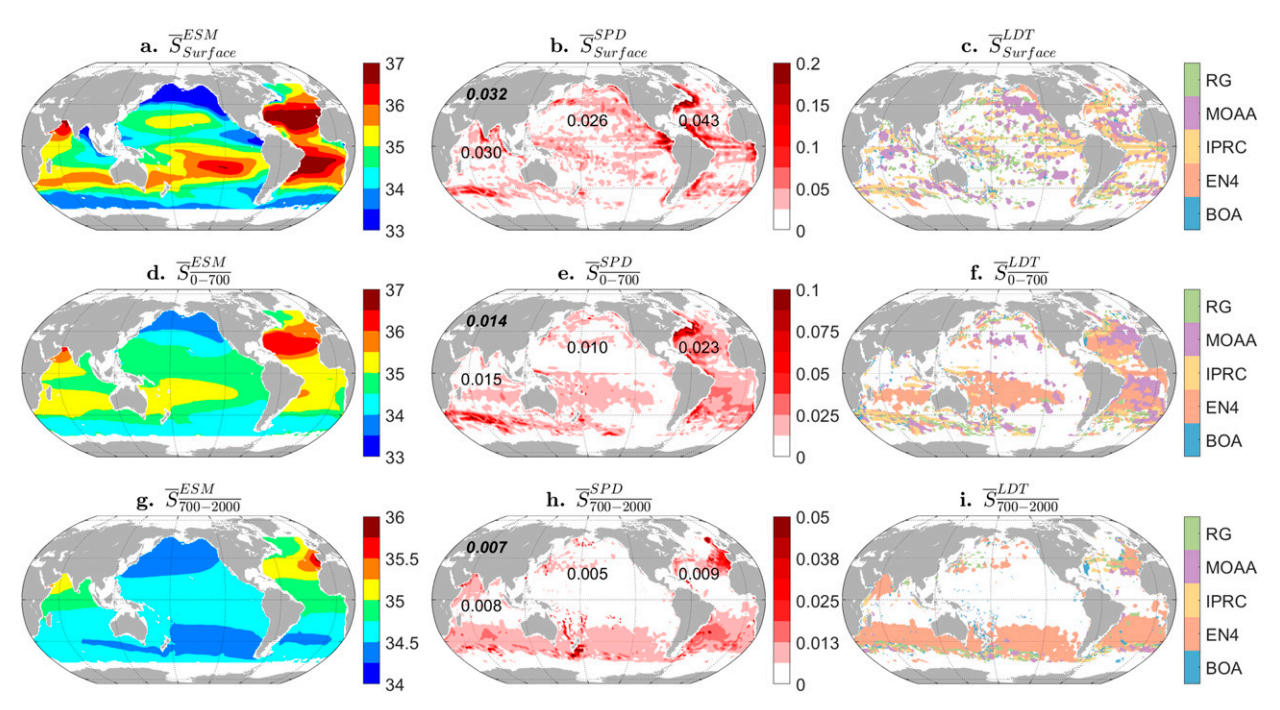


FIG. 2. Distribution of (left) the ensemble mean of the temporally averaged salinity over 2005–15 (\overline{S}^{ESM}), (center) its ensemble spread (\overline{S}^{SPD}), and (right) largest deviation (\overline{S}^{LDT}) for (a)–(c) sea surface, (d)–(f)0–700 m, and (g)–(i) 700–2000 m. The regular-font numbers in the \overline{S}^{SPD} panels indicates the area mean of each basin, and the bold italic number is its global mean. The \overline{S}^{LDT} panels only depict the sources of the deviations that are larger than 1/8 of \overline{S}^{SPD} maximum, not the actual values.

equivalent to the "truth" due to the spatially and temporally uneven distribution of Argo floats and low number of samples averaged.

3. Results

a. Mean state

The spatial patterns of \overline{S}^{ESM} , the temporally averaged ocean salinity (\overline{S}) , are presented in Fig. 2 together with the corresponding \overline{S}^{SPD} and \overline{S}^{LDT} . The geographical patterns of salinity for the surface and subsurface layers are evidently different (Fig. 2, left column). The pattern of sea surface salinity (SSS), which is strongly affected by the air-sea freshwater exchange (Yu 2011), is strongly zonal (Fig. 2a). Basin-scale patches can be found in the vertically averaged salinity (Figs. 2d,g) and roughly reflect the spatial distribution of the subsurface water masses. We can clearly see the relatively freshwater in the North Pacific and the Southern Ocean, and the highly saline Mediterranean Outflow Water, which is an important modulator of the North Atlantic salt budget below 700 m (Voelker et al. 2006). Overall, the 0–700 and 700–2000 m vertically averaged salinity distribution shows a combination of a large range of factors, including various forms of mode, intermediate, and deep water masses.

Although regional features of \overline{S} are generally robust among the products, the distribution of \overline{S}^{SPD} (Fig. 2, center column) shows that the discrepancies on climatological mean often exceed 0.02 for the surface, and 0.01 for the subsurface. At the surface, high values of \overline{S}^{SPD} appear in the major ocean current systems (e.g., the Gulf Stream, the Eastern Equatorial Countercurrent, and the Agulhas Return Current), where mesoscale eddies and sharp salinity fronts are challenging to resolve with Argo floats (Fig. 2b). These regions are also poorly sampled in general (Vinogradova et al. 2019), and the sparse observations can lead to high sampling errors in the mapping process (Kosempa and Chambers 2016). Similar differences are found in the 0-700 m and the 700-2000 m layers, except that values of \overline{S}^{SPD} are smaller by a factor of 2–3. Overall, the sampling errors associated with sparse float observations introduce large uncertainties into the products analvzed in the current study.

Values of $\overline{S}^{\text{LDT}}$ (Fig. 2, right column) and the differences of \overline{S} between each gridded product and $\overline{S}^{\text{ESM}}$ (Fig. 3) provide further information on the discrepancies. For instance, one of the largest deviations at the surface comes from IPRC (Fig. 2c). The zonal pattern in the IPRC residuals (Fig. 3j) is likely due to the use of an absolute dynamic height model (ADH), which can be viewed as a streamfunction of

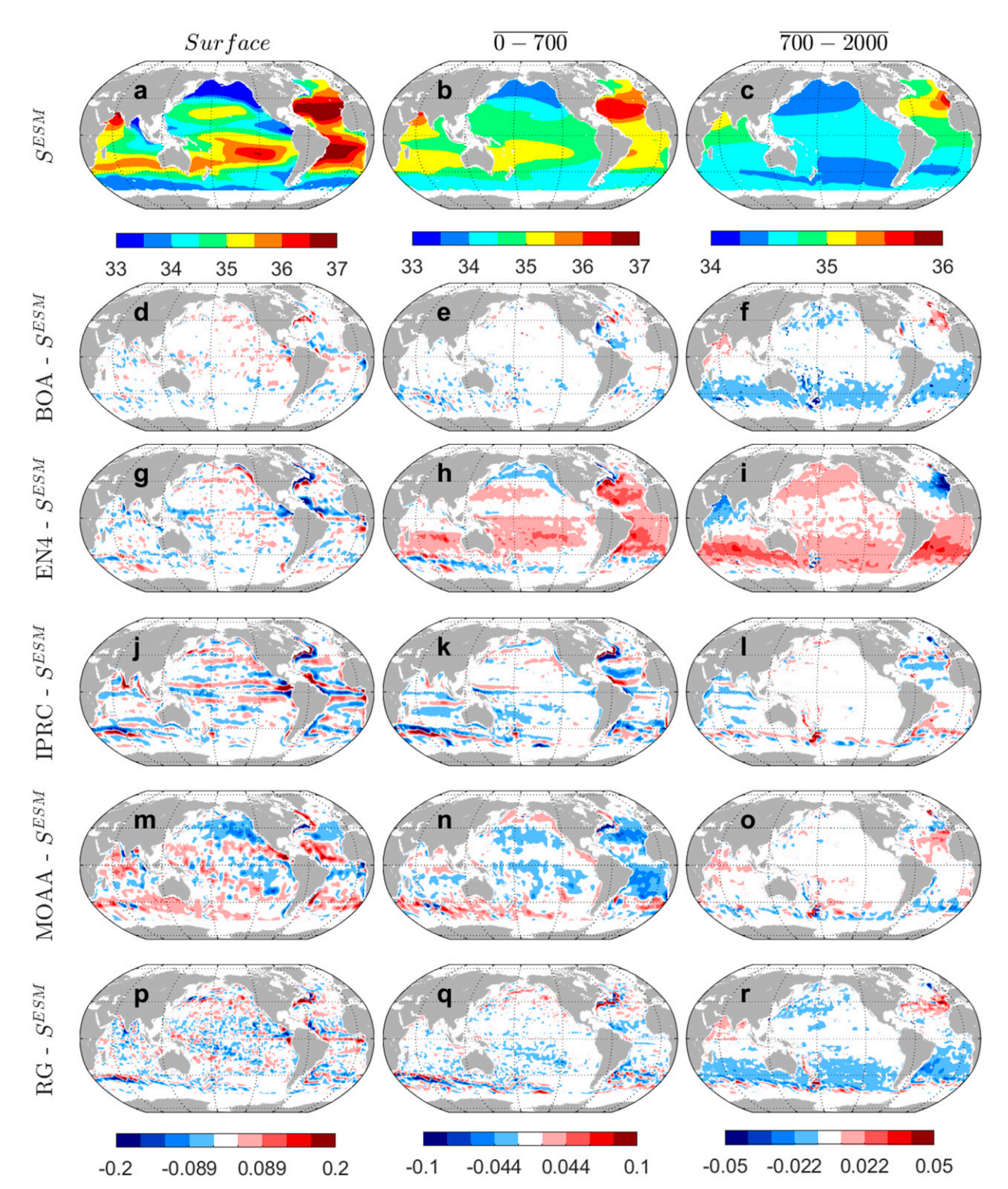


FIG. 3. Comparison of (a)–(c) \overline{S}^{ESM} and (d)–(r) the deviations of each gridded product from S_{ESM} for different layers. Shown are BOA, EN4, IPRC, MOAA, and RG for (left) sea surface, (center) 0–700 m, and (right) 700–2000 m.

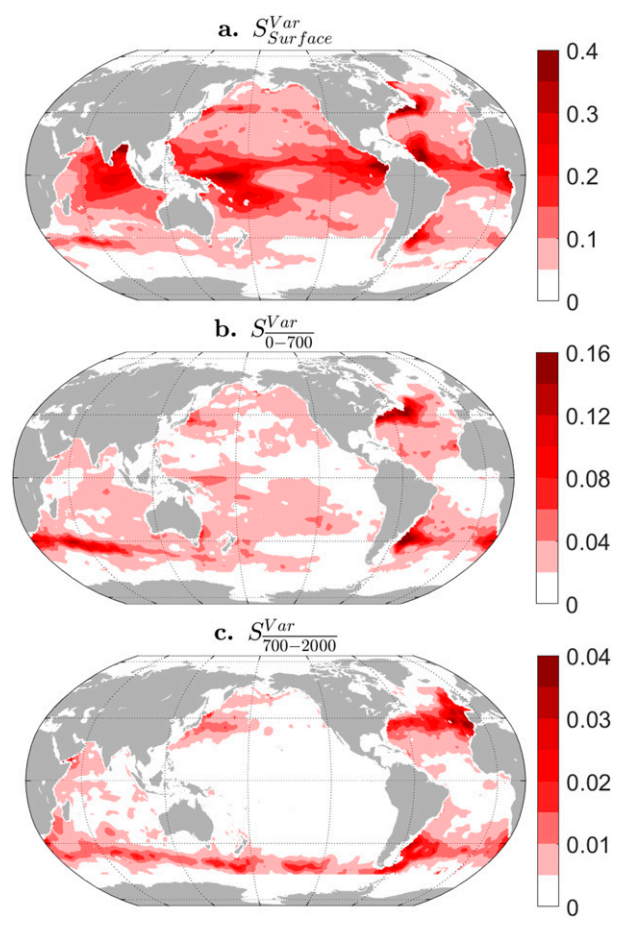


FIG. 4. Salinity variability (S^{Var}) from S^{ESM} for (a) sea surface and the (b) 0–700 and (c) 700–2000 m layers.

geostrophic circulation; shifts in strength and position of zonal currents will influence the three-dimensional spatial grid.

In comparison, EN4 and MOAA show large-scale deviations in the subsurface layers (e.g., Figs. 2f and 2i). These deviations highlight the importance of data selection and choice of climatological field (the "first guess") since EN4 and MOAA are the only two products applying pre-Argo baseline climatology. More specifically, the baseline climatology of EN4 approximately represents the average over 1971–2000 with a mean time in 1985 with sparse observations, which is approximately 25 years older than that of RG and BOA. Such difference on baseline climatology can lead to large-scale bias (Figs. 3g-i). For instance, the disagreements in the North Atlantic between EN4 and SESM are likely due to the 25-yr older climatology introducing signals of a different phase of the Atlantic multidecadal variability (Stendardo et al. 2016; Zhang et al. 2019). However, it is still elusive why MOAA shows a large-scale opposite pattern to EN4 while both share similar data sources and baseline climatology.

Discrepancies are also apparent in the temporal variability of salinity, which is further explored in the next section. The geographical patterns of salinity variability $(S^{\text{Var}}; \text{ calculated as the temporal standard deviation of }$ the S^{ESM} time series) in different layers of the global ocean are presented in Fig. 4. The value of S^{Var} is high where one would expect, in areas of strong freshwater exchanges and dynamical processes. For instance, at the sea surface, the east and west boundaries of the tropical Atlantic are modulated by major river runoffs, and the Indonesian Seas by the air-sea freshwater exchange. The western boundary currents and the Antarctic Circumpolar Current also contribute to S^{Var} , especially for the subsurface ocean. As the patterns of S^{Var} largely resemble the patterns of \overline{S}^{SPD} (Fig. 2, center column), it further supports that the discrepancies of climatological mean salinity are closely related to the temporal variability of salinity.

b. Temporal variability

1) SALINITY CHANGES IN DIFFERENT OCEAN LAYERS

Figure 5 shows the time series of the anomaly of global-averaged salinity $(\langle S' \rangle)$ for the sea surface, upper 700 m, and 700–2000 m layer from 2005 to 2015. While there is no significant trend in any layer, $\langle S' \rangle$ varies on different time scales ranging from seasonal to interannual. For instance, $\langle S' \rangle$ at the sea surface (Fig. 5a) shows strong interannual variability, which has a modest negative correlation (around -0.4) with the Multivariate ENSO Index (MEI) for the 10-yr period. A similar relationship between halosteric sea level and ENSO has been reported before (e.g., Fasullo et al. 2013; Wang et al. 2017). In addition, such interannual variability can also be inferred from the GRACE-based ocean mass change (Llovel et al. 2019), although the spatial coverage of GRACE is slightly different from that of most gridded Argo products used in this study.

The five products in general show similar salinity changes both at the sea surface (correlation around 0.95) and in the subsurface (correlation around 0.8). Although substantial discrepancies are visible (especially from MOAA and EN4 in 2005), $\langle S' \rangle^{SPD}$ (dashed line in Fig. 5) is below 0.01 most of the time. However, since the subsurface salinity changes are also below 0.01 and on the same order of magnitude, these discrepancies point to substantial uncertainty in these estimates. Notably, $\langle S' \rangle^{\text{LDT}}$ (colored bar in Fig. 5) shows that RG salinity values deviate from other datasets and S_{ESM} in 2008-09 and 2014-15 at the sea surface, and the second half of 2015 in the 700-2000 m layer. A similar deviation of RG is found before in halosteric sea level studies (Wang et al. 2017). In addition, MOAA deviates from most products in 2006-07 and 2011-15 below 700 m; further analysis (Fig. 100) shows it mostly comes from the tropical Pacific

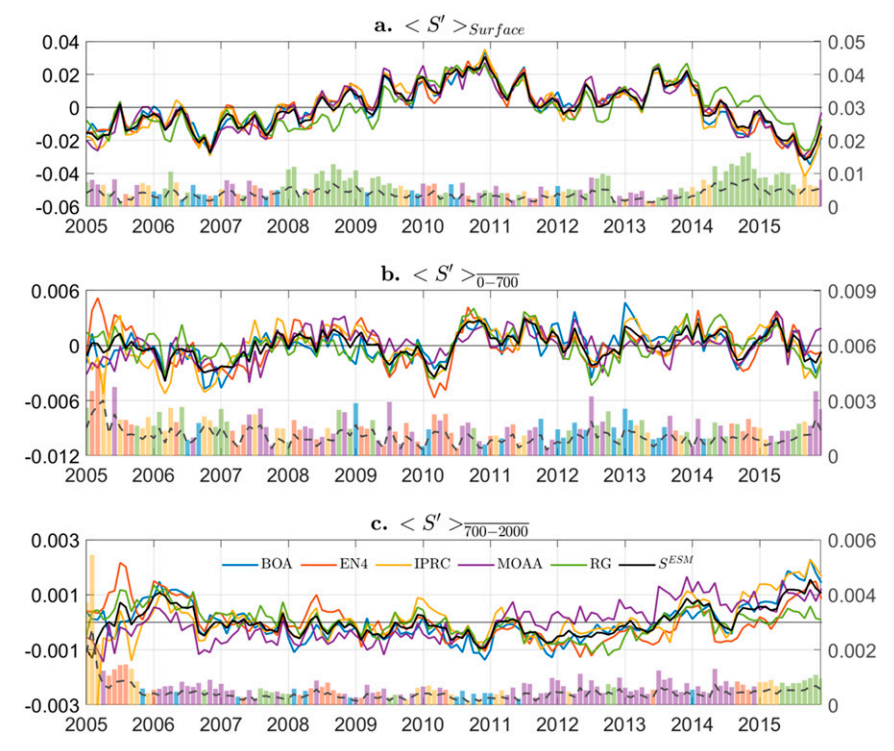


FIG. 5. Anomaly of monthly and globally averaged salinity ($\langle S' \rangle$, left axis) for different layers. Shown are BOA, EN4, IPRC, MOAA, RG, and S^{ESM} for (a) sea surface, (b) 0–700 m, and (c) 700–2000 m. The dashed line and the colored bars at the bottom of each panel are the ensemble spread ($\langle S' \rangle^{\text{SPD}}$) and the largest deviation ($\langle S' \rangle^{\text{LDT}}$) for each month. Values for both $\langle S' \rangle^{\text{SPD}}$ and $\langle S' \rangle^{\text{LDT}}$ are given on the right axis. The color scheme for $\langle S' \rangle$ and $\langle S' \rangle^{\text{LDT}}$ are the same.

Ocean. These discrepancies profoundly impact the estimated long-term trends with these products (see section 3c).

Another interesting feature in Fig. 5 is that $\langle S' \rangle^{SPD}$ and $\langle S' \rangle^{\text{LDT}}$ do not show any noticeable trend; both parameters declined in 2005 and then stayed constant. In comparison, the Argo array achieved quasi-global coverage in 2005, and the number of the deployed floats increased stably without drastic rate of change (Johnson et al. 2015; Wijffels et al. 2016; Riser et al. 2016; Boyer et al. 2018). On the one hand, the steady $\langle S' \rangle^{\text{SPD}}$ implies that all mapping methods used by the five datasets can generate robust salinity fields on the global scale based on available salinity profiles. On the other hand, the fact that $\langle S' \rangle^{\text{SPD}}$ does not change much with the increasing number of observations indicates the development of $1^{\circ} \times 1^{\circ}$ global ocean objective analyses may have encountered some limits. Products with higher resolution (e.g., Cabanes et al. 2013; Kolodziejczyk et al. 2017) may be needed to better utilize the increasing surface and subsurface measurements, which will greatly benefit studies on ocean fronts, mesoscale eddies, and other oceanic processes.

Salinity changes over time are further analyzed at different depths (Figs. 6 and 7). For the upper 700 m layer, strong interannual variability appears in the mixed layer and travels

downward to about 200 m within approximately 1.5 years (Fig. 6a). Meanwhile, $\langle S' \rangle_{0-700}^{\rm SPD}$ and $\langle S' \rangle_{0-700}^{\rm LDT}$ (Figs. 6c,e) show that the salinity profiles for EN4 largely deviate from other datasets in the upper 100 m (Fig. 1), mostly due to their different vertical resolutions and sources of data. Below 700 m, there are also interannual variations in salinity, although the magnitude is smaller than 0.005. Similarly, due to the differences in vertical spacing and bias from other assimilated data, large discrepancies appear below 700 m in 2006, 2008, 2011, and 2015. Figure 7 further compares the deviations of each dataset from S^{ESM}. Figures 6f and 7f suggest that EN4 is likely the leading cause for most of the high $\langle S' \rangle_{700-2000}^{SPD}$. Disagreements on long-term trends also appear, as Figs. 7j and 7l show a salinity increase for MOAA and a decrease for RG relative to SESM for the 700-2000 m layer. Furthermore, an annually recurring residual signal is found between 800 and 1000 m for IPRC, (Fig. 7h), which will be further explored in the next section.

2) TIME EVOLUTION OF ZONAL MEAN SALINITY

Analysis of zonal means can provide further information about the temporal variability of salinity on the global scale (Figs. 8a–c). The zonal mean of SSS anomaly $(\langle S'_{\text{Zonal}} \rangle_{\text{Surface}})$ shows significant semiannual variability at

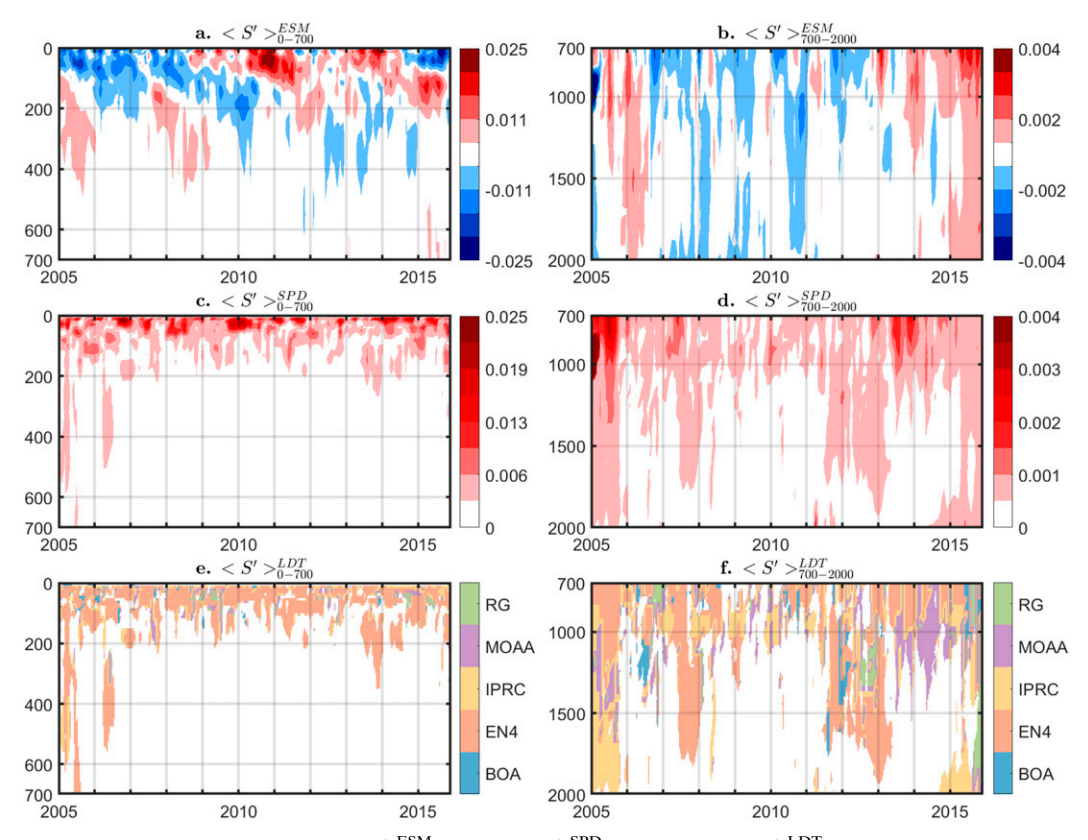


FIG. 6. Time evolution of (top) $\langle S' \rangle^{\text{ESM}}$, (middle) $\langle S' \rangle^{\text{SPD}}$, and (bottom) $\langle S' \rangle^{\text{LDT}}$ for (a),(c),(e) 0–700 and (b),(d),(f) 700–2000 m. The $\langle S' \rangle^{\text{LDT}}$ panels only depict the sources of the deviations that are larger than 1/8 of $\langle S' \rangle^{\text{SPD}}$ maximum, not the actual values.

all latitudes and long-term trends in the midlatitudes (Fig. 8a). For instance, a negative trend is found in 40°–60°N, which can be attributed to the accelerated hydrological cycle (Durack et al. 2012). On the basin scale (not shown), the freshening is most prominent in the North Atlantic, which is likely due to a decline in the meridional salt transport (Robson et al. 2016; Tesdal et al. 2018).

Another major feature is the interannual variability in the tropical region (30°S–30°N), which comes from the Pacific Ocean and propagates away from the equator. This pattern is closely linked to ENSO through the common EOF analyses (next paragraph).

For the upper 700 m layer (Fig. 8b), the pattern of $\langle S'_{\rm Zonal} \rangle_{\overline{0-700}}$ is similar to that of $\langle S'_{\rm Zonal} \rangle_{\rm Surface}$ but of smaller magnitude and much weaker interannual variability. Below 700 m, the spatial structure of $\langle S'_{\rm Zonal} \rangle_{\overline{700-2000}}$ consists of an interannual fluctuation between 40°-60°N and 30°-50°S and a long-term salinification between 30°S and 40°N (Fig. 8c).

While the differences between the various datasets and S^{ESM} in their zonal means (Figs. 8d-i) are very subtle, the common EOF analyses of the time series of the zonal mean salinity reveal some robust and inconsistent features (Fig. 9). At the sea surface, the

first and second EOF modes account for about 45% of the total variance. The spatial pattern of mode 1 (Fig. 9a) shows a minimum located in the tropical region (10°S-20°N) and two peaks centered at 15°S and 30°N, and the PC from S^{ESM} (Fig. 9b) has a modest correlation with MEI (dashed line in Fig. 9b) at 0.69 for the period 2005-15. The correlation coefficient increases if $\langle S'_{\rm Zonal} \rangle_{\rm Surface}$ is calculated in the Pacific Ocean (0.74) instead of the global ocean, especially for the band 20°S-20°N (0.85). Since ENSO originates in the tropical Pacific with significant regional impacts, it largely modulates the salinity changes in that region (e.g., Hackert et al. 2011; Zhu et al. 2014; Zheng and Zhang 2015; Zhao et al. 2016). Therefore, the first EOF mode of zonal mean SSS anomaly is dominated by the variability associated with ENSO. The second mode shows a different spatial structure (Fig. 9c): the spatial pattern between the equator and 30°N is positive, while the subpolar region north to 40°N is negative. As the PC steadily increases from 2005 to 2015 (Fig. 9d), mode 2 likely represents positive trends centered at 20°N and 40°S, which are prominent in the Pacific Ocean, and a negative trend between 40°-60°N in the North Atlantic (Fig. 10a). Previous studies (Vinogradova and Ponte 2017; Li et al. 2019) show

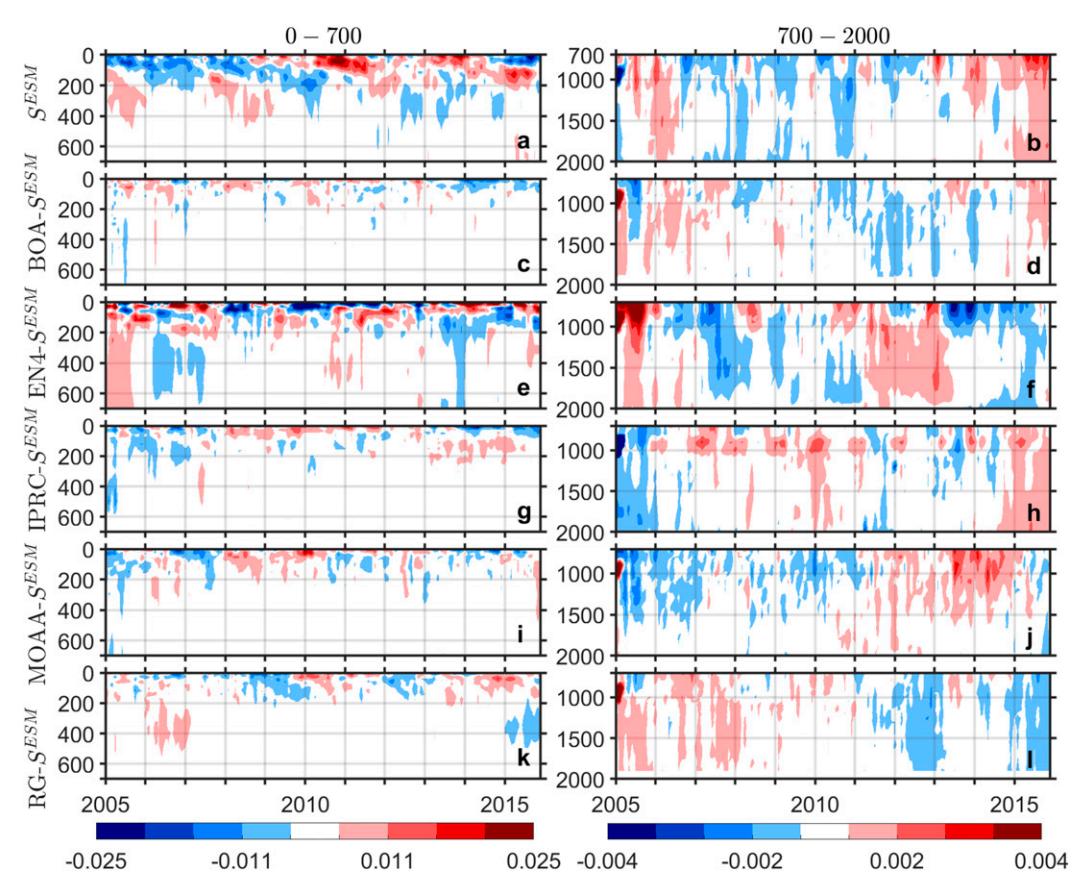


FIG. 7. A comparison of (a),(b) $\langle S' \rangle^{\text{ESM}}$ and (c)–(l) the deviations of each gridded product from S_{ESM} for different layers. Shown are BOA, EN4, IPRC, MOAA, and RG for (left) 0–700 and (right) 700–2000 m.

that the increase of salinity in the Pacific Ocean was mainly caused by a reduction of surface precipitation and is related to the interdecadal Pacific oscillation (IPO).

For the 0–700 m layer, mode 1 of $\langle S'_{Zonal} \rangle_{\overline{0-700}}$ and mode 2 of $\langle S'_{Zonal} \rangle_{Surface}$ have similar structures and PCs, as do mode 2 of $\langle S'_{Zonal} \rangle_{\overline{0-700}}$ and mode 1 of $\langle S'_{Zonal} \rangle_{Surface}$ (Figs. 9e–h). Mode 1 represents a positive decadal trend at 20°N and 40°S, and a negative trend between 40°–60°N (Figs. 9e,f). Mode 2 shows an ENSO-like pattern (Figs. 9g,h), and the PC from S^{ESM} is correlated with MEI at 0.74.

Below 700 m, the results are not as robust as for the surface and the upper 700 m. The strongest signals in mode 1 are in the subpolar regions of the Northern Hemisphere (Fig. 9i). This peak corresponds to the Mediterranean outflow region, where the temporal variability is stronger than in the rest of the ocean (Fig. 4c). The PCs represent an interannual anomaly for most products that is positive in 2006–07 and negative in 2010–11 (Fig. 9j). In addition, the second EOF mode (Figs. 9k,l) explains 17% of the observed variance depending on the datasets.

The EOF results also highlight the differences in the interpretation of interannual variability in different

products, especially for the 700-2000 m layer. For instance, MOAA shows disagreements from others in the Northern Hemisphere in mode 1, and RG largely disagrees with most products in mode 2. Moreover, the first two modes of $\langle S'_{\text{Zonal}} \rangle_{\overline{700-2000}}$ from IPRC are visibly different from other products. Based on the peak at about 30°N and its seasonal variation, mode 1 of IPRC likely represents the recurring residual signal in Fig. 7h. Mode 2 of IPRC is similar to mode 1 of other products (Figs. 9k,l) but with a broader peak. In addition, the annually recurring residual from IPRC reappears in Fig. 8f, and is located in the North Atlantic, approximately at 30°N, 25°W in the Mediterranean outflow region. The source of these signals is the local data availability in the IPRC salinity product at 900 and 1000 m depth in certain years. Due to the location and regularity, the reported residual occurs in our intercomparison of global and zonal means.

c. Global and regional salinity trends over 2005–15

Discrepancies in the mean salinity over the global ocean can heavily affect the estimation of long-term

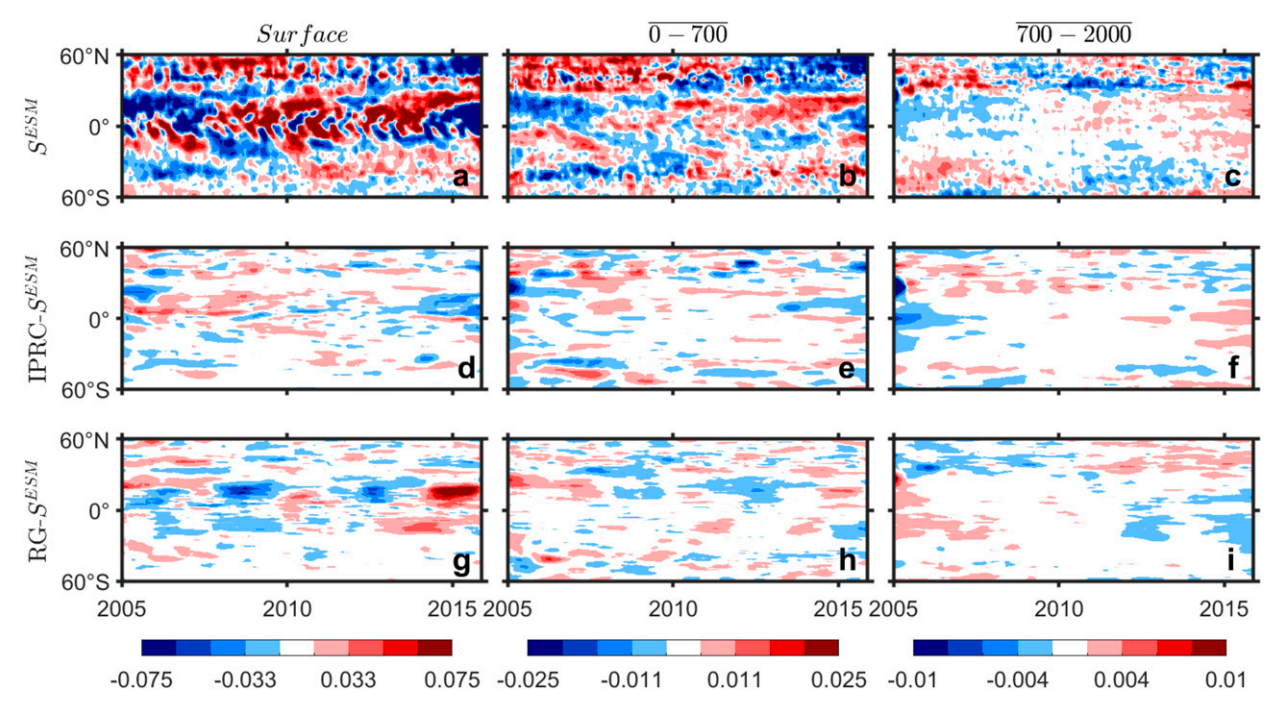


FIG. 8. A comparison of (a)–(c) zonal mean salinity anomalies ($\langle S'_{Zonal} \rangle^{ESM}$) and (d)–(i) the deviations of selected gridded products from S^{ESM} for different layers. Shown are IPRC and RG for (left) sea surface, (center) 0–700 m, and (right) 700–2000 m after a 7-month running mean.

trends both globally and regionally, especially if those differences are not random. To better illustrate these discrepancies, the linear trend of the salinity time series is calculated conventionally by generalized least squares regression (Table 1). In this analysis, the trends are calculated for the period 2006–14 after removing the seasonality, and we assume random residuals and account for reduced degrees of freedom. The uncertainties of these trends are also provided at the 90% confidence level.

The estimated trend of sea surface salinity ($\langle S' \rangle_{Surfac}^{TND}$ varies from insignificant value of $1.28 \pm 2.52 \times 10^{-3} \text{ yr}^{-1}$ for IPRC to $1.90 \pm 2.32 \times 10^{-3}$ for IPRC to $1.90 \pm 2.33 \times 10^{-3} \text{yr}^{-1}$ for MOAA, while the RG surface salinity is significant at 3.01 \pm 1.99 \times $10^{-3}\,\mathrm{yr}^{-1}$. However, it is worth noting that $\langle S' \rangle_{\mathrm{Surface}}^{\mathrm{TND}}$ from RG is not significantly different from other datasets accounting for their overlaps within the uncertainties. For the upper 700 m layer, all salinity trends are positive with large uncertainties so that ranges include zero. Trends in the 700–2000 m layer ($\langle S' \rangle_{700-2000}^{TND}$) vary from $-0.27 \pm 1.01 \times 10^{-4} \text{yr}^{-1}$ for BOA to $-0.09 \pm 0.87 \times$ 10^{-4}yr^{-1} for S_{ESM} . Among the products, EN4, MOAA, and RG show a trend that is significantly different from zero $(-1.15 \pm 1.02 \times 10^{-4}, 1.68 \pm 0.68 \times 10^{-4}, \text{ and } -0.81 \pm$ $0.76 \times 10^{-4} \text{yr}^{-1}$, respectively), but they do not agree in terms of sign. In addition, the entire upper 2000 m also does not present any significant trend.

Regionally, changes in ocean salinity will affect the local buoyancy balance, stratification, and the derived halosteric heights (Durack et al. 2014; Llovel and Lee 2015; Wang et al. 2017; Tesdal et al. 2018). In contrast to the trends in the global mean salinity, the spatial patterns of regional salinity trends (S^{TND}) are similar among all products (Fig. 10). At the sea surface (Fig. 10, left column), the salinity increased in the subtropical Pacific but decreased in the North Atlantic and the eastern Indian Ocean. The increase in the Pacific is induced by the reduction of precipitation (Li et al. 2019), and the decrease in the North Atlantic is the result of an increase of the freshwater input from the Arctic (e.g., Proshutinsky et al. 2009; Tesdal et al. 2018). The freshening in the eastern Indian Ocean is likely related to the Indian Ocean dipole (IOD; Huang et al. 2008) and the strengthening of the Indonesian Throughflow with enhanced regional precipitation (Llovel and Lee 2015).

For the upper 700 m layer (Fig. 10, center column), the pattern of S_{0-700}^{TND} largely resembles that of $S_{Surface}^{TND}$ with similar major patches of significant increases and decreases, but the estimated trend values are about 50% smaller. Compared to $S_{Surface}^{TND}$, one of the unique features of S_{0-700}^{TND} is the salinification in the subtropical Atlantic, which is likely due to the changes in the Mediterranean outflow since 2005 (Schroeder et al. 2016). In addition, S_{0-700}^{TND} from MOAA and RG are visibly smaller than

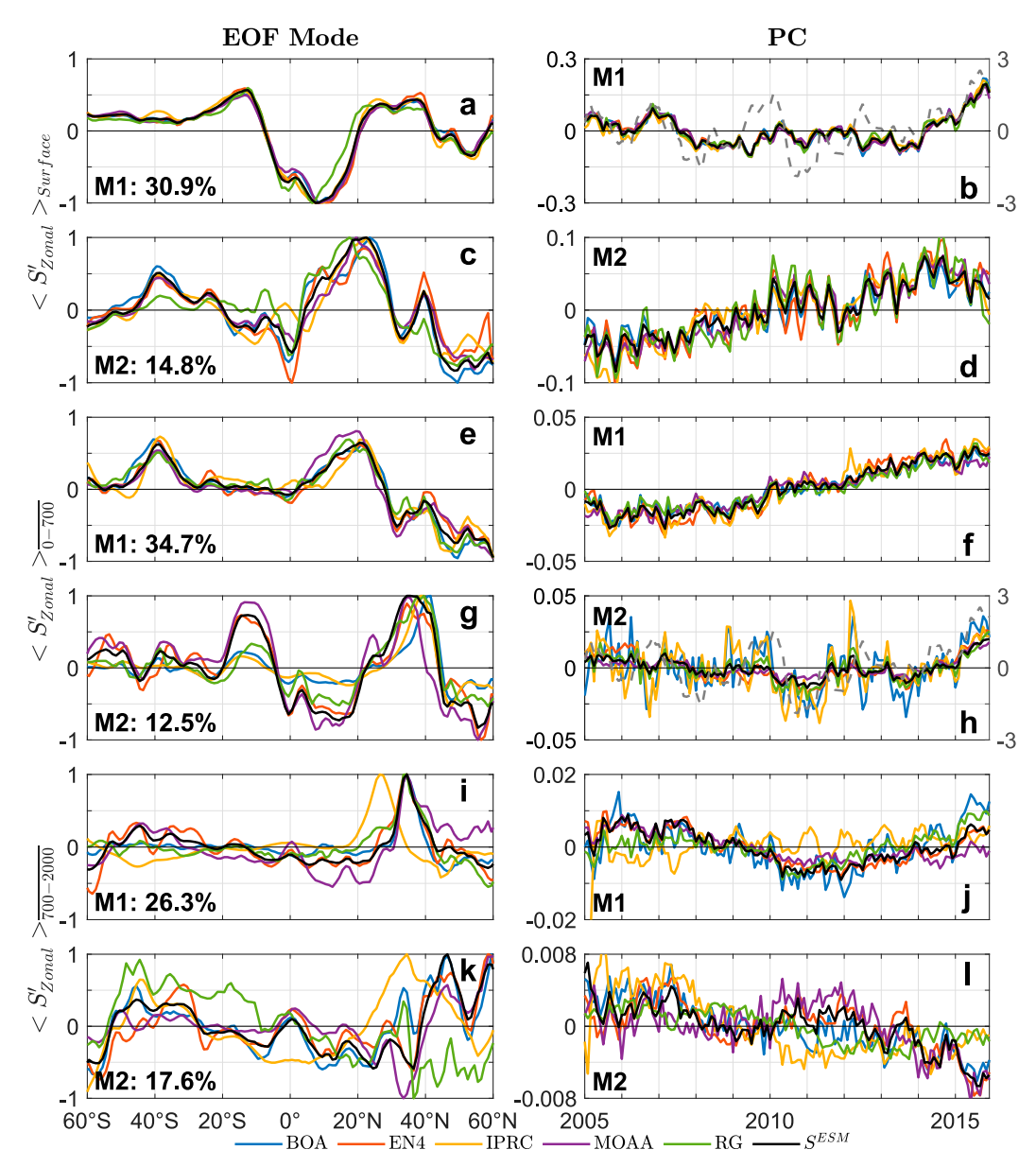


FIG. 9. First and second EOF modes of $\langle S'_{\text{Zonal}} \rangle$ for (a)–(d) sea surface, (e)–(h) 0–700 m, and (i)–(l) 700–2000 m. Shown are (left) the spatial structures and (right) the principal components for BOA, EN4, IPRC, MOAA, RG, and S^{ESM} . The dashed line in (b) and (h) is the MEI (see the right axis). The mean fraction of variance explained by each EOF mode is also provided.

other products, although they agree after accounting for the uncertainties (Figs. 10n,q).

For the 700–2000 m layer, some large-scale features (e.g., salinification in the Pacific and the polar front, freshening in the Atlantic) are still robust (Fig. 10, right column); the South Atlantic and the subpolar regions are freshening, and the salinity is increasing slowly in the tropical Pacific. Such regional patterns are consistent with other studies based on different measurements and reanalysis products (e.g., Robson et al. 2016; Giglio and Johnson 2016, 2017; Tesdal et al. 2018). In general, deep

water movements in the North Atlantic (Buckley and Marshall 2016) and the north Indian Ocean (Thompson et al. 2016) increase the salinity variability. Due to stronger temporal variability, sampling and interpolation errors are expected to be larger. Meanwhile, the patterns of $S_{700-2000}^{\text{TND}}$ from BOA, EN4, and RG (Figs. 10f,i,r) are substantially scattered in the tropical region. In addition, most products present a large-scale freshening in the Sargasso Sea, but RG shows a smaller value (Fig. 10r).

The most apparent discrepancy for the 700– $2000\,\mathrm{m}$ layer occurs in the tropical region. A positive trend in the tropical

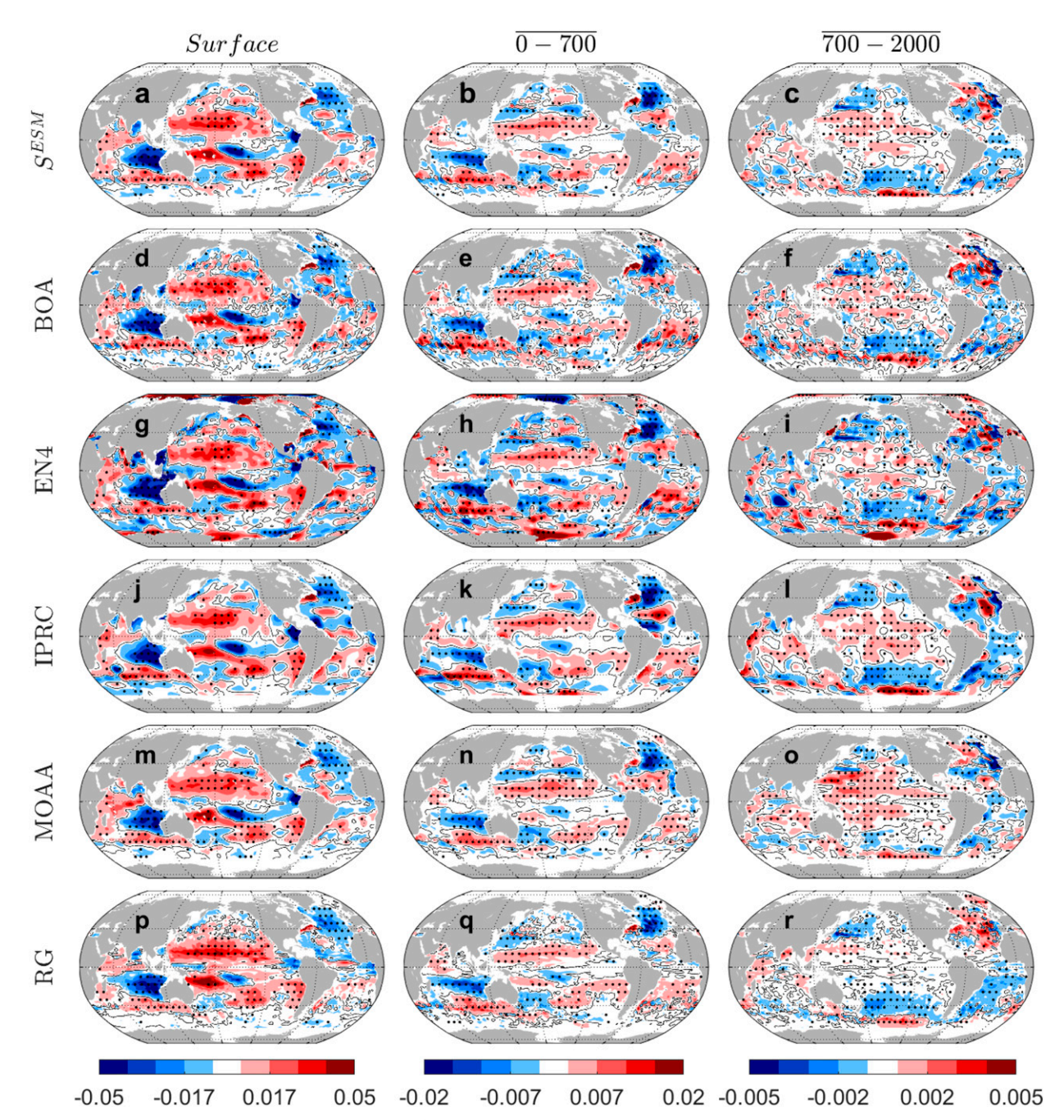


FIG. 10. Spatial pattern of salinity trend (S^{TND} ; yr $^{-1}$) from (top to bottom) S^{ESM} , BOA, EN4, IPRC, MOAA, and RG over 2005–15 for (left) sea surface, (center) 0–700 m, and (right) 700–2000 m. Black contours mark zero. Stippling indicates areas of statistically significant nonzero values at the 90% confidence level.

Pacific appears in all products except RG (Fig. 10r), where the salinity change is visibly smaller. Between 25°S and 25°N, nearly all the products suggest a more saline tropical Pacific since 2005. The estimated trend for the regional area-averaged salinity (Table 1) ranges from $2.33 \times 10^{-4} \, \mathrm{yr}^{-1}$ for EN4 to $5.87 \times 10^{-4} \, \mathrm{yr}^{-1}$ for MOAA with relatively small uncertainty (0.56–1.24 \times $10^{-4} \, \mathrm{yr}^{-1}$). However, the RG

salinity trend is much smaller and insignificant at $0.23 \pm 0.79 \times 10^{-4} \, \mathrm{yr}^{-1}$. Also, RG has the lowest regional spatial correlation to S^{ESM} at 0.6, while that of other products is 0.7–0.9. Interestingly, better agreement on the salinity trend for the global ocean can be achieved after excluding the tropical Pacific (summarized in Table 1): most of the Argo-based OA products show significant freshening ranging

TABLE 1. Decadal trends of salinity in different layers of the global ocean from each individual dataset and ensemble mean $(\times 10^{-4}\,\mathrm{yr}^{-1})$. Regional [tropical Pacific (Tropical Pac.) and global ocean excluding tropical Pacific (Global excl. TP)] trends in the 0–2000 m layer are also given. Uncertainties are estimated at the 90% confidence level. Bold indicates the result is significantly different from zero.

	BOA	EN4	IPRC	MOAA	RG	S^{ESM}
Global trend						
Sea surface	14.6 ± 24.0	17.5 ± 24.3	12.8 ± 25.2	19.0 ± 23.3	30.1 ± 19.9	18.8 ± 24.2
0-700 m	2.84 ± 1.81	1.89 ± 3.30	2.68 ± 3.23	0.95 ± 1.65	1.69 ± 2.21	2.01 ± 2.15
700–2000 m	-0.27 ± 1.01	-1.15 ± 1.02	0.08 ± 0.73	1.68 ± 0.68	-0.81 ± 0.76	-0.09 ± 0.87
0-2000 m	-0.11 ± 0.94	-0.92 ± 1.30	0.13 ± 1.13	0.80 ± 0.69	-1.31 ± 1.17	-0.24 ± 1.07
Regional trend in the	e 700–2000 m layer					
Tropical Pac.	2.88 ± 1.24	2.33 ± 1.14	5.03 ± 0.56	5.87 ± 0.78	0.23 ± 0.79	3.24 ± 0.59
Global exc. TP	-1.53 ± 0.95	-2.51 ± 0.91	-1.92 ± 0.80	-0.03 ± 0.81	-1.18 ± 1.08	-1.44 ± 0.97

from $-2.51 \pm 0.91 \times 10^{-4} \text{yr}^{-1}$ (EN4) to $-1.18 \pm 1.08 \times 10^{-4} \text{yr}^{-1}$ (RG), except MOAA ($-0.03 \pm 0.81 \times 10^{-4} \text{yr}^{-1}$), which shows less of a decrease in the Southern Ocean and Indian Ocean as displayed in Fig. 10o.

4. Summary

In this study, we compared salinity around the global ocean from five Argo-based gridded products to present the robust salinity variability over 2005–15. We also identified the discrepancies associated with individual products and presented some evidence for the sources of these differences. As prior studies indicate (e.g., Boyer et al. 2016; Wang et al. 2017), a large portion of these differences relates to the choice of mapping method, baseline climatology, and data correction (Domingues et al. 2008; Ishii and Kimoto 2009; Levitus et al. 2012; Abraham et al. 2013; Chang et al. 2013; Boyer et al. 2016). The impacts of those factors are evident in our estimation of the time mean, temporal variability, and decadal trends of global ocean salinity.

The time mean of ocean salinity is overall robust, both on values and spatial distributions. Small but detectable discrepancies (around 0.02) appear mostly in regions that are either dynamically active or have large salinity gradients (e.g., the Gulf Stream and the Agulhas Return Current). These active conditions are challenging for sampling and further interpolation, resulting in large uncertainties. The choice of mapping methods and baseline climatology could also cause nonnegligible disagreements. For instance, the banded pattern from IPRC residuals (Figs. 3j,k) is likely related to its interpolation method, in which an ADH model is additionally applied onto the three-dimensional grid. EN4 and MOAA, the only two objective analyses that used pre-Argo data as the baseline climatology, also exhibit basin-scale deviations. While further work is needed to better understand these discrepancies and uncertainties, it is recommended to be careful choosing the best climatology for the well-observed Argo era.

Temporal variability of salinity over the global ocean were then assessed on different spatial scales. In general, many variations are robust: strong interannual variability is evident in the upper ocean with a downward propagation; the patterns of zonal evolution show impact of ENSO and a combination of long-term trends at different latitudes. Apart from these robust features, subtle discrepancies were also revealed and can be attributed to the data source. One example is that EN4 and MOAA, the only two products that utilized non-Argo data, deviate from the others on the global mean below 700 m during the first few years of the examined period. Meanwhile, IPRC shows a recurring annual residual around 900 m in the North Atlantic due to the lack of data in its gridded salinity product. These disagreements on subsurface salinity anomalies are at least comparable to the anomalies themselves, indicating the importance of improving the in situ measurements since such large uncertainties discourage any meaningful interpretation.

The global and regional salinity trends were also examined over the 10-yr period. For the global mean, while the trend values are unanimously positive for the sea surface and the upper 700 m layer, no statistically significant trends can be concluded at any examined layer for their large uncertainties. In contrast to the global mean, patterns of the regional salinity trends are highly robust among different products. Large-scale disagreements only arise in the tropical Pacific and the Southern Ocean, and the most evident deviation comes from RG, in which smaller trends prevail in almost the entire tropical Pacific. The source of this basin-scale deviation remains elusive, but it is in line with previous studies that show the RG salinity has been drifting at least since 2015 (e.g., Wang et al. 2017), which would cause smaller overall trends. It is unclear if this observed deviation in the 700–2000 m layer is associated with the

recently reported drifting (Roemmich et al. 2019). In addition, our results show a consistent freshening over the global ocean if the tropical Pacific is excluded.

5. Discussion

Overall, while some of the revealed discrepancies among these OA products are equal to or smaller than those of the ocean reanalyses when comparing to prior studies (e.g., Shi et al. 2017), they do reveal potential issues that need attention. The spatial and temporal variability of global ocean salinity described in this study provide an opportunity to examine changes in water cycle, especially the change in ocean mass. Although no significant trends in the global mean salinity were identified in any of the examined layers, the prevailing positive trend values in the upper 700 m ocean are evident. In particular, such a salinification is not in line with recent estimates of freshwater discharges that are based on GRACE measurements (Llovel et al. 2019). Some studies (Wang et al. 2017) suggest the observed trends could be caused by not properly accounting for the effects of freshwater input in inadequately sampled regions, contributions from the deep ocean, and changes in surface forcing and interannual variability which dominate the trends over the examined period. Further investigations are still needed to fully address this disagreement.

As some gridded products (e.g., EN4) are evidently different from the others on subsurface salinity variability, the use of the ensemble mean can represent an optimal scenario with reduced bias (e.g., Shi et al. 2017; Toyoda et al. 2017; Wang et al. 2017). At present, intercomparison studies on temperature and heat content are regularly conducted, and similar studies on salinity should be carried out in the future as well.

One interesting finding of this study is that the discrepancies among the examined products do not decrease with the increase of salinity observations from the Argo program. For instance, some of the observed discrepancies on the global mean salinity are an obvious result of inadequate sampling (e.g., the deviation of EN4 and IPRC in global mean salinity in the early 2000s). However, in regions and periods that are sampled with greatly improved coverage, substantial disagreements are also observed and some can be largely attributed to the differences in mapping methods (Boyer et al. 2016). Beside the suspicious deviation of RG from other gridded products since 2015, such discrepancies among the gridded products are concerning. Therefore, better ways are needed to utilize the increasing Argo profiles as merely increasing the number of Argo profiles does not necessarily improve the consistency between these $1^{\circ} \times 1^{\circ}$ gridded products.

Moreover, high-resolution products are also necessary to study mesoscale and submesoscale oceanic structures.

In short, there is still much work to be done to improve the estimation and interpretation of observed salinity variations over the global ocean. The present effort is a useful step toward improving the understanding of the uncertainties in salinity variability during the Argo period. Our results provide helpful guidance on the use of current gridded Argo products by many researchers in their own studies and serve as a useful reference for data centers working on the development of next-generation gridded Argo products.

Acknowledgments. The authors are grateful for the editor and two anonymous reviewers for their constructive comments. The work was supported in part by the National Science Foundation through Grant OCE-2021274 and the National Aeronautics and Space Administration through Grant 80NSSC20K0752. Support from the GRACE Follow-On Science Team through Grant 80NSSC20K0728 (RMP) is also acknowledged. The Argo data were collected and made freely available by the International Argo Program and the national programs that contribute to it (http://www.argo.ucsd.edu; http://argo.jcommops.org). The Argo Program is part of the Global Ocean Observing System.

REFERENCES

- Abraham, J. P., and Coauthors, 2013: A review of global ocean temperature observations: Implications for ocean heat content estimates and climate change. *Rev. Geophys.*, **51**, 450–483, https://doi.org/10.1002/rog.20022.
- Argo, 2000: Argo float data and metadata from Global Data Assembly Centre (Argo GDAC). SEANOE, accessed August 2018, https://doi.org/10.17882/42182.
- Balmaseda, M. A., and Coauthors, 2015: The Ocean Reanalyses Intercomparison Project (ORA-IP). J. Oper. Oceanogr., 8, S80–S97, https://doi.org/10.1080/1755876x.2015.1022329.
- Barnes, S. L., 1964: A technique for maximizing details in numerical weather map analysis. *J. Appl. Meteor.*, **3**, 396–409, https://doi.org/10.1175/1520-0450(1964)003<0396:ATFMDI>2.0.CO;2.
- Boyer, T. P., S. Levitus, J. I. Antonov, R. A. Locarnini, and H. E. Garcia, 2005: Linear trends in salinity for the World Ocean, 1955–1998. *Geophys. Res. Lett.*, 32, L01604, https://doi.org/10.1029/2004GL021791.
- —, and Coauthors, 2016: Sensitivity of global upper-ocean heat content estimates to mapping methods, XBT bias corrections, and baseline climatologies. *J. Climate*, 29, 4817–4842, https:// doi.org/10.1175/JCLI-D-15-0801.1.
- —, and Coauthors, 2018: World Ocean Database 2018. A. Mishonov, Technical Ed., NOAA Atlas NESDIS 87, https://data.nodc.noaa.gov/woa/WOD/DOC/wod_intro.pdf.
- Buckley, M. W., and J. Marshall, 2016: Observations, inferences, and mechanisms of the Atlantic meridional overturning circulation: A review. *Rev. Geophys.*, 54, 5–63, https://doi.org/10.1002/2015RG000493.

- Cabanes, C., and Coauthors, 2013: The CORA dataset: Validation and diagnostics of in-situ ocean temperature and salinity measurements. Ocean Sci., 9, 1–18, https://doi.org/10.5194/os-9-1-2013.
- Chang, Y.-S., S. Zhang, A. Rosati, T. L. Delworth, and W. F. Stern, 2013: An assessment of oceanic variability for 1960–2010 from the GFDL ensemble coupled data assimilation. *Climate Dyn.*, 40, 775–803, https://doi.org/10.1007/s00382-012-1412-2.
- Curry, R., B. Dickson, and I. Yashayaev, 2003: A change in the freshwater balance of the Atlantic Ocean over the past four decades. *Nature*, 426, 826–829, https://doi.org/10.1038/nature02206.
- Domingues, C., J. Church, N. White, P. Gleckler, S. Wijffels, P. Barker, and J. Dunn, 2008: Improved estimates of upperocean warming and multi-decadal sea-level rise. *Nature*, 453, 1090–1093, https://doi.org/10.1038/nature07080.
- Dong, C., J. C. McWilliams, Y. Liu, and D. Chen, 2014: Global heat and salt transports by eddy movement. *Nat. Commun.*, 5, 3294, https://doi.org/10.1038/ncomms4294.
- Durack, P. J., 2015: Ocean salinity and the global water cycle. Oceanography, 28, 20–31, https://doi.org/10.5670/oceanog.2015.03.
- —, and S. E. Wijffels, 2010: Fifty-year trends in global ocean salinities and their relationship to broad-scale warming. *J. Climate*, 23, 4342– 4362, https://doi.org/10.1175/2010JCLI3377.1.
- —, and R. J. Matear, 2012: Ocean salinities reveal strong global water cycle intensification during 1950 to 2000. Science, 336, 455–458, https://doi.org/10.1126/science.1212222.
- —, and P. J. Gleckler, 2014: Long-term sea-level change revisited: The role of salinity. *Environ. Res. Lett.*, 9, 114017, https://doi.org/10.1088/1748-9326/9/11/114017.
- Fasullo, J. T., C. Boening, F. W. Landerer, and R. S. Nerem, 2013: Australia's unique influence on global sea level in 2010–2011. Geophys. Res. Lett., 40, 4368–4373, https://doi.org/10.1002/grl.50834.
- Foltz, G. R., S. A. Grodsky, J. A. Carton, and M. J. McPhaden, 2004: Seasonal salt budget of the northwestern tropical Atlantic Ocean along 38°W. J. Geophys. Res., 109, C03052, https://doi.org/10.1029/2003JC002111.
- Giglio, D., and G. C. Johnson, 2016: Subantarctic and polar fronts of the Antarctic Circumpolar Current and Southern Ocean heat and freshwater content variability: A view from Argo. J. Phys. Oceanogr., 46, 749–768, https://doi.org/10.1175/JPO-D-15-0131.1.
- —, and —, 2017: Middepth decadal warming and freshening in the South Atlantic. J. Geophys. Res. Oceans, 122, 973–979, https://doi.org/10.1002/2016JC012246.
- Good, S. A., M. J. Martin, and N. A. Rayner, 2013: EN4: Quality controlled ocean temperature and salinity profiles and monthly objective analyses with uncertainty estimates. *J. Geophys. Res. Oceans*, 118, 6704–6716, https://doi.org/10.1002/2013jc009067.
- Hackert, E., J. Ballabrera-Poy, A. J. Busalacchi, R. H. Zhang, and R. Murtugudde, 2011: Impact of sea surface salinity assimilation on coupled forecasts in the tropical Pacific. *J. Geophys. Res.*, 116, C05009, https://doi.org/10.1029/2010JC006708.
- Haumann, F., and Coauthors, 2016: Sea-ice transport driving Southern Ocean salinity and its recent trends. *Nature*, 537, 89– 92, https://doi.org/10.1038/nature19101.
- Helm, K. P., N. L. Bindoff, and J. A. Church, 2010: Changes in the global hydrological-cycle inferred from ocean salinity. *Geophys. Res. Lett.*, 37, L18701, https://doi.org/10.1029/2010GL044222.
- Hosoda, S., T. Ohira, and T. Nakamura, 2008: A monthly mean dataset of global oceanic temperature and salinity derived from Argo float observations. *JAMSTEC Rep. Res. Dev.*, 8, 47–59, https://doi.org/10.5918/jamstecr.8.47.

- —, T. Suga, N. Shikama, and K. Mizuno, 2009: Global surface layer salinity change detected by Argo and its implication for hydrological cycle intensification. *J. Oceanogr.*, 65, 579–586, https://doi.org/10.1007/s10872-009-0049-1.
- Huang, B., Y. Xue, and D. W. Behringer, 2008: Impacts of Argo salinity in NCEP Global Ocean Data Assimilation System: The tropical Indian Ocean. *J. Geophys. Res.*, 113, C08002, https://doi.org/10.1029/2007JC004388.
- IPRC, 2019: IPRC products based on Argo data. International Pacific Research Center, accessed 26 April 2019, http:// apdrc.soest.hawaii.edu/projects/argo/.
- Ishii, M., and M. Kimoto, 2009: Reevaluation of historical ocean heat content variations with time-varying XBT and MBT depth bias corrections. *J. Oceanogr.*, 65, 287–299, https:// doi.org/10.1007/s10872-009-0027-7.
- Jayne, S. R., D. Roemmich, N. Zilberman, S. C. Riser, K. S. Johnson, G. C. Johnson, and S. R. Piotrowicz, 2017: The Argo program present and future. *Oceanography*, 30, 18–28, https://doi.org/10.5670/oceanog.2017.213.
- Johnson, G. C., J. M. Lyman, and S. G. Purkey, 2015: Informing deep Argo array design using Argo and full-depth hydrographic section data. *J. Atmos. Oceanic Technol.*, 32, 2187– 2198, https://doi.org/10.1175/JTECH-D-15-0139.1.
- Kolodziejczyk, N., P.-M. Annaig, and G. Fabienne, 2017: ISAS-15 temperature and salinity gridded fields. SEANOE, accessed March 2019, https://doi.org/10.17882/52367.
- Kosempa, M., and D. P. Chambers, 2016: Mapping error in Southern Ocean transport computed from satellite altimetry and Argo. J. Geophys. Res. Oceans, 121, 8063–8076, https:// doi.org/10.1002/2016JC011956.
- Lee, T., 2016: Consistency of Aquarius sea surface salinity with Argo products on various spatial and temporal scales. *Geophys. Res. Lett.*, **43**, 3857–3864, https://doi.org/10.1002/2016GL068822.
- Levitus, S., J. I. Antonov, T. P. Boyer, H. E. Garcia, and R. A. Locarnini, 2005: Linear trends of zonally averaged thermosteric, halosteric, and total steric sea level for individual ocean basins and the world ocean, (1955–1959)–(1994–1998). *Geophys. Res. Lett.*, 32, L16601, https://doi.org/10.1029/2005GL023761.
- —, and Coauthors, 2012: World ocean heat content and thermosteric sea level change (0–2000 m), 1955–2010. Geophys. Res. Lett., 39, L10603, https://doi.org/10.1029/2012GL051106.
- Li, G., Y. Zhang, J. Xiao, X. Song, J. Abraham, L. Cheng, and J. Zhu, 2019: Examining the salinity change in the upper Pacific Ocean during the Argo period. *Climate Dyn.*, 53, 6055– 6074, https://doi.org/10.1007/s00382-019-04912-z.
- Li, H., F. H. Xu, W. Zhou, D. X. Wang, J. S. Wright, Z. H. Liu, and Y. L. Lin, 2017: Development of a global gridded Argo data set with Barnes successive corrections. *J. Geophys. Res. Oceans*, **122**, 866–889, https://doi.org/10.1002/2016JC012285.
- Liu, C., and Coauthors, 2019: Vertical redistribution of salt and layered changes in global ocean salinity. *Nat. Commun.*, 10, 3445, https://doi.org/10.1038/s41467-019-11436-x.
- Llovel, W., and T. Lee, 2015: Importance and origin of halosteric contribution to sea level change in the southeast Indian Ocean during 2005–2013. *Geophys. Res. Lett.*, 42, 1148–1157, https:// doi.org/10.1002/2014GL062611.
- —, B. Meyssignac, and A. Cazenave, 2011: Steric sea level variations over 2004.2010 as a function of region and depth: Inference on the mass component variability in the North Atlantic Ocean. *Geophys. Res. Lett.*, 38, L15608, https://doi.org/10.1029/2011GL047411.

- —, and Coauthors, 2019: Global ocean freshening, ocean mass increase and global mean sea level rise over 2005–2015. *Sci. Rep.*, **9**, 17717, https://doi.org/10.1038/s41598-019-54239-2.
- Proshutinsky, A., and Coauthors, 2009: Beaufort Gyre freshwater reservoir: State and variability from observations. J. Geophys. Res., 114, C00A10, https://doi.org/10.1029/2008JC005104.
- Purkey, S. G., G. C. Johnson, and D. P. Chambers, 2014: Relative contributions of ocean mass and deep steric changes to sea level rise between 1993 and 2013. *J. Geophys. Res. Oceans*, 119, 7509–7522, https://doi.org/10.1002/2014JC010180.
- Rao, R. R., and R. Sivakumar, 2003: Seasonal variability of sea surface salinity and salt budget of the mixed layer of the North Indian Ocean. *J. Geophys. Res.*, 108, 3009, https://doi.org/ 10.1029/2001JC000907.
- Riser, S. C., and Coauthors, 2016: Fifteen years of ocean observations with the global Argo array. *Nat. Climate Change*, **6**, 145–153, https://doi.org/10.1038/nclimate2872.
- Robson, J., P. Ortega, and R. Sutton, 2016: A reversal of climatic trends in the North Atlantic since 2005. *Nat. Geosci.*, 9, 513– 517, https://doi.org/10.1038/ngeo2727.
- Roemmich, D., and J. Gilson, 2009: The 2004–2008 mean and annual cycle of temperature, salinity, and steric height in the global ocean from the Argo Program. *Prog. Oceanogr.*, 82, 81–100, https://doi.org/10.1016/j.pocean.2009.03.004.
- —, and Coauthors, 2009: The Argo Program: Observing the global ocean with profiling floats. *Oceanography*, 22, 34–43, https://doi.org/10.5670/oceanog.2009.36.
- —, and Coauthors, 2019: On the future of Argo: A global, full-depth, multi-disciplinary array. Front. Mar. Sci., 6, 439, https://doi.org/10.3389/fmars.2019.00439.
- Schmitt, R. W., 2008: Salinity and the global water cycle. *Oceanography*, 21, 12–19, https://doi.org/10.5670/oceanog.2008.63.
- Schroeder, K., and Coauthors, 2016: Abrupt climate shift in the western Mediterranean Sea. Sci. Rep., 6, 23009, https://doi.org/ 10.1038/srep23009.
- Shi, L., and Coauthors, 2017: An assessment of upper ocean salinity content from the Ocean Reanalyses Intercomparison Project (ORA-IP). Climate Dyn., 49, 1009–1029, https://doi.org/10.1007/ s00382-015-2868-7.
- Skliris, N., and Coauthors, 2014: Salinity changes in the World Ocean since 1950 in relation to changing surface freshwater fluxes. *Climate Dyn.*, **43**, 709–736, https://doi.org/10.1007/s00382-014-2131-7.
- Stendardo, I., M. Rhein, and R. Hollmann, 2016: A high resolution salinity time series 1993–2012 in the North Atlantic from Argo and altimeter data. *J. Geophys. Res. Oceans*, **121**, 2523–2551, https://doi.org/10.1002/2015JC011439.
- Storto, A., and Coauthors, 2017: Steric sea level variability (1993–2010) in an ensemble of ocean reanalyses and objective analyses. Climate Dyn., 49, 709–729, https://doi.org/10.1007/s00382-015-2554-9.
- Tesdal, J. E., R. P. Abernathey, J. I. Goes, A. L. Gordon, and T. W. Haine, 2018: Salinity trends within the upper layers of the subpolar North Atlantic. *J. Climate*, 31, 2675–2698, https://doi.org/10.1175/JCLI-D-17-0532.1.
- Thompson, P. R., C. G. Piecuch, M. A. Merrifield, J. P. McCreary, and E. Firing, 2016: Forcing of recent decadal variability in the

- equatorial and north Indian Ocean. *J. Geophys. Res. Oceans*, **121**, 6762–6778, https://doi.org/10.1002/2016JC012132.
- Toyoda, T., and Coauthors, 2017: Intercomparison and validation of the mixed layer depth fields of global ocean syntheses. *Climate Dyn.*, **49**, 753–773, https://doi.org/10.1007/s00382-015-2637-7.
- Trenberth, K. E., J. T. Fasullo, K. von Schuckmann, and L. Cheng, 2016: Insights into Earth's energy imbalance from multiple sources. J. Climate, 29, 7495–7505, https://doi.org/10.1175/JCLI-D-16-0339.1.
- Vinogradova, N. T., and R. M. Ponte, 2017: In search of fingerprints of the recent intensification of the ocean water cycle. *J. Climate*, 30, 5513–5528, https://doi.org/10.1175/JCLI-D-16-0626.1.
- —, and Coauthors, 2019: Satellite salinity observing system: Recent discoveries and the way forward. *Front. Mar. Sci.*, **6**, 243, https://doi.org/10.3389/fmars.2019.00243.
- Voelker, A. H. L., S. M. Lebreiro, J. Schönfeld, I. Cacho, H. Erlenkeuser, and F. Abrantes, 2006: Mediterranean outflow strengthening during northern hemisphere coolings: A salt source for the glacial Atlantic? *Earth Planet. Sci. Lett.*, 245, 39–55, https://doi.org/10.1016/j.epsl.2006.03.014.
- von Schuckmann, K., and P. Y. Le Traon, 2011: How well can we derive global ocean indicators from Argo data? *Ocean Sci.*, **7**, 783–791, https://doi.org/10.5194/os-7-783-2011.
- Wang, G. J., L. J. Cheng, T. Boyer, and C. Y. Li, 2017: Halosteric sea level changes during the Argo era. Water, 9, 484, https:// doi.org/10.3390/w9070484.
- —, L. Cheng, J. Abraham, and C. Li, 2018: Consensuses and discrepancies of basin-scale ocean heat content changes in different ocean analyses. *Climate Dyn.*, 50, 2471–2487, https:// doi.org/10.1007/s00382-017-3751-5.
- Wijffels, S., and Coauthors, 2016: Ocean temperatures chronicle the ongoing warming of Earth. *Nat. Climate Change*, 6, 116– 118, https://doi.org/10.1038/nclimate2924.
- Xue, Y., and Coauthors, 2012: A comparative analysis of upperocean heat content variability from an ensemble of operational ocean reanalyses. *J. Climate*, 25, 6905–6929, https:// doi.org/10.1175/JCLI-D-11-00542.1.
- —, and Coauthors, 2017: A real-time ocean reanalyses intercomparison project in the context of tropical Pacific observing system and ENSO monitoring. *Climate Dyn.*, 49, 3647–3672, https://doi.org/10.1007/s00382-017-3535-y.
- Yu, L. S., 2011: A global relationship between the ocean water cycle and near-surface salinity. J. Geophys. Res., 116, C10025, https://doi.org/10.1029/2010JC006937.
- Zhang, R., and Coauthors, 2019: A review of the role of the Atlantic meridional overturning circulation in Atlantic multidecadal variability and associated climate impacts. *Rev. Geophys.*, 57, 316–375, https://doi.org/10.1029/2019RG000644.
- Zhao, M., H. H. Hendon, Y. H. Yin, and O. Alves, 2016: Variations of upper-ocean salinity associated with ENSO from PEODAS reanalyses. J. Climate, 29, 2077–2094, https://doi.org/10.1175/ JCLI-D-15-0650.1.
- Zheng, F., and R. H. Zhang, 2015: Interannually varying salinity effects on ENSO in the tropical Pacific: A diagnostic analysis from Argo. *Ocean Dyn.*, 65, 691–705, https://doi.org/10.1007/ s10236-015-0829-7.
- Zhu, J. S., B. H. Huang, R. H. Zhang, Z. Z. Hu, A. Kumar, M. A. Balmaseda, L. Marx, and J. L. Kinter, 2014: Salinity anomaly as a trigger for ENSO events. *Sci. Rep.*, **4**, 6821, https://doi.org/10.1038/srep06821.